HHS Public Access

Author manuscript

Nat Biomed Eng. Author manuscript; available in PMC 2017 December 30.

Published in final edited form as:

Nat Biomed Eng. 2017 ; 1: . doi:10.1038/s41551-017-0094.

Microscale arrays for the profiling of start and stop signals coordinating human-neutrophil swarming

Eduardo Reátegui[1,2,3], **Fatemeh Jalali**[1], **Aimal H. Khankhel**[1,2], **Elisabeth Wong**[1], **Hansang Cho**[1,3], **Jarone Lee**[3,4], **Charles N. Serhan**[3,5], **Jesmond Dalli**[3,5], **Hunter Elliott**[3,6], and **Daniel Irimia**[1,3,7]

[1]BioMEMS Resource Center, Department of Surgery, Massachusetts General Hospital

[2]Massachusetts General Hospital Cancer Center

[3]Harvard Medical School

[4]Department of Surgery, Massachusetts General Hospital

[5]Center for Experimental Therapeutics, Department of Anesthesiology, Perioperative, and Pain Medicine, Brigham and Women's Hospital

[6]Image and Data Analysis Core (IDAC)

[7]Shriners Burns Hospital

Abstract

Neutrophil swarms protect healthy tissues by sealing off sites of infection. In the absence of swarming, microbial invasion of surrounding tissues can result in severe infections. Recent observations in animal models have shown that swarming requires rapid neutrophil responses and well-choreographed neutrophil migration patterns. However, in animal models physical access to the molecular signals coordinating neutrophil activities during swarming is limited. Here, we report the development and validation of large microscale arrays of zymosan-particle clusters for the study of human neutrophils during swarming ex vivo. We characterized the synchronized swarming of human neutrophils under the guidance of neutrophil-released chemokines, and measured the mediators released at different phases of human-neutrophil swarming against targets

Correspondence and requests for materials to Daniel Irimia, dirimia@mgh.harvard.edu.

Code availability

The computer code for chemotaxis analysis and diffusion modeling is available in Github at https://github.com/hunterelliott/ChemotaxisModelling

Data availability

The authors declare that all data supporting the findings of this study are available within the paper and its supplementary information. Source data for the figures in this study are available in figshare with the identifier doi:10.6084/m9.figshare.5024567 (ref. 45).

Author contributions

E. R. and D. I. designed research. E. R., A. H. K., F. J., H. C. and E. W. designed and prepared microfluidic devices. E. R. conducted experiments. E. R., F. J., H. E., J. L. and D. I. analyzed results. C. N. S. and J. D. performed metabololipidomic analysis. H. E. developed the biophysical model for cell swarming. E. R. and D. I. prepared the manuscript, with significant contributions from all authors.

Competing financial interests

The authors declare no competing financial interests.

simulating infections. We found that the network of mediators coordinating human-neutrophil swarming includes start and stop signals, proteolytic enzymes and enzyme inhibitors, as well as modulators of activation of other immune and non-immune cells. We also show that the swarming behavior of neutrophils from patients following major trauma is deficient and gives rise to smaller swarms than those of neutrophils from healthy individuals.

Neutrophils represent the largest population of white blood cells in circulation. They are the first to accumulate in tissues after injury, infections, or inflammation. They are capable of swarming, a process by which they insulate areas of infection and injury from surrounding viable tissues, thus playing key roles in protecting the body from microbial infections and inflammation. Growing evidence of neutrophils swarming around microbes and damaged cells challenges the current paradigm regarding neutrophil accumulation under the exclusive control of chemoattractants released by microbes and tissue damage [1,2]. A new paradigm is emerging where neutrophils are active players, participating in their own recruitment [3]. Studies in mice have recently identified leukotriene B4 (LTB_4) as the "unique intercellular communication signal between neutrophils" for the recruitment of cells during swarming [2]. At the same time, a role for other chemokines and receptors during the aggregation phase of swarming has been proposed, supported by evidence from knockouts for single receptor genes [2,4]. However, the poor control over the conditions in tissues and the challenges of measuring inter-cellular molecular signals are significant barriers for dissecting the complexity of the neutrophil interactions during the different phases of swarming in vivo [1,2]. In addition, it is not clear whether the mechanisms identified in mice [1,2] could be directly extrapolated to human neutrophils, because of known differences in migration and chemokine responses between human and mouse neutrophils [5]. Even though neutrophil swarming has been observed *in vitro* around dying cells [6], no experimental system today can perform the precise and high-throughput characterization of human neutrophil swarming necessary to accelerate our understanding of the swarming processes and its mediators.

The well-choreographed recruitment of neutrophils by swarming is a key determinant for limiting the extent of infections with various pathogens[7]. Examples, supported by in vivo observations in animal models, include the neutrophil response to *Staphylococcus aureus* [8,9], *Escherichia coli* [10], *Listeria monocytogenes* [10], or *Toxoplasma gondii* [11]. Moreover, swarming contributes to effective responses to filamentous fungi like Aspergillus [12,13]. Unlike the typical chemotaxis of cells towards sources of diffusing attractant molecules, neutrophil swarming is characterized by an early, progressively accelerated, exponential accumulation of neutrophils at sites of infection or injury. The process is tightly controlled and stops promptly once the infection and/or injury site has been insulated from the surrounding healthy tissue [4,7]. Deficiencies of attracting large numbers of neutrophils around Aspergillus conidia may be responsible for the progression of infections in patients during immunosuppressive therapy [13], and decreased ability to neutralize Staphylococcus following major trauma [14]. Swarming also reaches clinical relevance when neutrophil response and accumulation is excessive and leads to tissue destruction e.g. transient swarms during inflammation in the lungs [10] and inflammation flares around uric acid crystals during gout disease [15]. Therefore, interventions to modulate neutrophil swarming, by reducing it in

conditions of detrimental inflammation or enhancing it during certain infections, could amend the disease processes and potentially improve conditions in patients.

Here, we designed a microscale array of particle-clusters to control and monitor the swarming behavior of human neutrophils and performed a comprehensive study of the signals mediating interactions between human neutrophils during swarming. This microscale array of particle-clusters enables the detailed study of hundreds of neutrophil swarms, synchronized in time around large arrays of identical targets. We found that both the size and the spacing of particle-clusters are critical for triggering swarming neutrophil behavior. We also identified a constellation of 45 mediators released by human neutrophil during swarming and absent in controlled conditions. A complex picture is emerging for the communication between human neutrophils during swarming, comprising both lipid and protein that act as start and stop signals for neutrophils, as well as mediators for the activities of monocytes, lymphocytes, and several non-inflammatory cells. Several mediators are apparently redundant and their contribution to swarming becomes important only when dominant ones are inhibited. Moreover, we tested the swarming ability of neutrophils in patients after trauma and found significant deficits that ameliorate during the hospital stay. A better understanding of the mediators of neutrophils swarming will ultimately enhance our abilities to control infections and chronic inflammation in patients.

Results

Requirements for neutrophil swarming on microscale array of particle clusters

We manufactured large-scale arrays of clusters of zymosan particles by first micropatterning a cationic copolymer polyelectrolyte of acrylamide (ZETAG® 8185) and then trapping precisely controlled numbers of negatively charged, micron-sized zymosan particles on top of these micropatterns (Fig. 1a, Supplementary Fig. 1). We produced targets of controlled size, dimensions, composition, and spacing, employed the arrays of zymosan-particle clusters as targets for human neutrophil accumulation. We observed that neutrophils converge towards particle clusters within minutes after loading the neutrophil suspension (Fig. 1b, c). In the presence of serum free media, the first neutrophils arrive to the targets by chance during the loading of the devices and subsequent neutrophils are guided by mediators released from the first cells. Human neutrophils formed swarms only around particle clusters larger than 17.5 μm^2 in size (more than 3 zymosan particles in a cluster) and spaced further than 20 μm distance from each other (Fig. 1d, Supplementary Fig. 2, Supplementary Video 1–3). Smaller clusters (1–2 zymosan particles), which were phagocytosed by individual neutrophils, did not induce swarming. Neutrophils colocalized above the smaller particle clusters and were employed as controls for the swarming experiments. Neutrophils placed on patterns in the absence of particles remained spherical and lacked evidence of activation (non-activated controls).

Swarming starts after neutrophils moving randomly on the surface of the microscale array encounter zymosan-particle clusters (*scouting phase* – represented as relative time 0 min, Fig. 1e). Within minutes after the initial interactions with particle clusters, increasing numbers of neutrophils start migrating towards the first neutrophils (*growth phase*). Swarms reach their maximum size at 40–70 minutes later, after which they stop growing (*plateau*

phase – Supplementary Table 1). During the plateau phase, neutrophils migrate in and out of the swarms, reflecting the dynamic nature of swarms at equilibrium. The assay is quantitative (Supplementary Fig. 3) and has high reproducibility, which we validated by comparing the swarming of neutrophils from the same donor in three separate assays (59.3 ± 8 μm^2 particle cluster size, 100 μm spacing, Fig. 1e). The differences between the dynamics of swarms in repeated experiments from the same donor are smaller than the differences between healthy donors (Fig. 1f).

Neutrophils can leave smaller swarms to join adjacent larger swarms. When zymosan-particle clusters of different size are spaced close together (distances between 40 and 60 μm), swarms around smaller clusters grow to a size that is on average one-third of the size of those around larger particle clusters (Fig. 1g, h). While the initial neutrophil recruitment occurs at the same rate on adjacent swarms, with time, swarms around smaller particle clusters reach the plateau phase and stop growing while swarms around larger clusters continue to grow. On average, two-dozen neutrophils leave each of the smaller swarms to join the adjacent larger swarms, increasing their size (Supplementary Fig. 4). When zymosan particle clusters of different size are positioned in arrays with spacing greater than 80 μm, they induce swarms of comparable size, even when particle clusters are up to twice the size of adjacent particle clusters. These observations show the presence of long-range interactions between adjacent swarms and indicate the presence of gradients of soluble mediators released from swarms, which guide the migration of neutrophils.

Several chemoattractants guide human neutrophil swarming

We verified that leukotriene B_4 (LTB_4), a signaling lipid playing a vital role during swarming in mice [2], is also mediating the swarming of human neutrophils. For this, we monitored neutrophil swarming in the presence of BLT1 and BLT2 receptor antagonists (U75302 and LY255283, Fig. 2a–d and 2e–h). We measured a reduction in the size of swarms in the presence of the antagonists (Fig. 2a, e). We measured a significant decrease in mean velocity of individual neutrophils migrating towards the swarms during the growth phase, from 15 μm/min in control conditions to 7 μm/min for neutrophils exposed to BLT1 and BLT2 receptor antagonists (Fig. 2b, c, f, g and Supplementary Fig. 5). It was interesting to note that the growth phase was significantly slower in the presence of BLT1 and BLT2 receptor antagonists. Neutrophil recruitment velocity was uniform over time, with no noticeable acceleration during the growth phase. The analysis of the trajectories of neutrophils joining the swarms also revealed significant changes. The chemotactic index (CI) decreased significantly, and migration patterns became disorganized in the presence of BLT1 and BLT2 receptor antagonists (CI = 0.5) compared to neutrophils in control conditions (CI = 0.94, Fig. 2d, h, Supplementary Fig. 4). Simultaneously, the radius of neutrophil recruitment was reduced from 300 ± 30 to 120 ± 30 μm ($n = 16$, $p < 0.05$). The average ratio between swarm and particle cluster size (δ_{Ratio}) was reduced from 2 ± 0.3× to 1.2 ± 0.2× ($n = 14$, $p < 0.05$, Fig. 2i, j). These results are in agreement with the *in vivo* measurements that showed that the recruitment of mouse neutrophils lacking LTB_4 receptors is drastically impaired [2]. Similar to the insights from mice, our results also suggest that additional chemoattractant signals, besides LTB_4, may contribute to the swarming of human neutrophils.

We guided our search for additional chemoattractants by employing a biophysical model to leverage the measured changes in the timing of motility initiation, the original location of neutrophils joining the swarms, and the characteristics of neutrophil movement in the vicinity of swarms (Supplementary Fig. 6). The model provided estimates of chemoattractant diffusivity and helped narrow the range of potential chemoattractants for neutrophils during swarming. We started by validating the biophysical model on human neutrophil swarming in control conditions. The results from the model were consistent with a chemoattractant that diffuses rapidly away from swarms ($1.2 \pm 0.4 \times 10^{-10}$ m^2/s) and the characteristic fast, persistent, and highly directional migration of human neutrophils in LTB_4 gradients [16] (Fig. 2k and 2l; experimental and simulation results, respectively. Supplementary Video 4). In the presence of BLT1 and BLT2 receptor antagonists, the results of the biophysical model were consistent with the activity of a chemoattractant with slower diffusivity ($0.6 \pm 0.4 \times 10^{-10}$ m^2/s) guiding the migration of neutrophils towards swarms. Moreover, the convoluted trajectories of neutrophils towards swarms and lower migration speed were consistent with the bi-directional signature motility patterns of neutrophils in the presence of CXCL8 and C5a chemoattractants [16]. Together, the results of the biophysical model and chemoattractant signatures support the involvement of additional chemoattractants, besides LTB_4, during human neutrophil swarming, with LTB_4 signaling reinforced by higher molecular weight chemoattractants (Fig. 2m and 2n; experimental and simulation results, respectively. Supplementary Video 5).

Guided by these experimental and biophysical modeling results, we probed the contribution of CXCL8 and heat-labile factors (e.g. complement) during neutrophil swarming (Fig. 3a, b). We compared the recruitment of neutrophils in the presence of regular ($CI = 0.94 \pm 0.04$) and heat-inactivated serum in the medium. In heat inactivated serum, we observed a reduction in the chemotactic index ($CI = 0.88 \pm 0.04$, $p < 0.05$) (Fig. 3c), a lower number of neutrophils in the plateau phase, and a less than 10 min delay before the establishment of a stable recruitment phase (Fig. 3d). The combination of BLT1 and BLT2 antagonists and heat-inactivated serum further reduced the recruitment of neutrophils to swarms (Fig. 3a, b, d). Together, these results indicate that heat-labile factors play a non-redundant role during swarming, and become important in the absence of LTB_4 mediated guidance. Moreover, we measured no decrease of the chemotactic index in the presence of CXCR1 and CXCR2 blocking antibodies ($CI = 0.87 \pm 0.04$) when compared to experiments in heat-inactivated serum. The chemotactic index decreased significantly when the blocking of BLT1 and BLT2 occurred in the presence of heat-inactivated serum ($CI = 0.74 \pm 0.04$, $p < 0.05$), and decreased even further with the additional blocking of CXCR1 and CXCR2($CI = 0.62 \pm 0.04$, $p < 0.05$, Fig. 3c). The number of neutrophils recruited to the swarms was further reduced when serum was replaced with human albumin, suggesting that other factors in serum contribute to swarming (Fig. 3e). Interestingly, despite being slowed significantly, neutrophil recruitment to the swarms was not completely abolished even after interference with all recruitment factors identified so far, including the LTB_4, CXCL8, and heat-labile serum factor(s) (Fig. 3d, e).

Lipid mediators of human neutrophil swarming

To identify additional signals, we probed the presence of other lipid mediators, besides LTB_4, in the supernatant and released by human neutrophils during swarming. Such measurements were enabled by the augmented concentration of mediators in the supernatant, favored by the synchronized release and the small volume of fluid above the swarms. We focused on the presence of lipid mediators of inflammation and resolution derived from arachidonic acid (AA), eicosapentaenoic acid (EPA), or docoshexaenoic acid (DHA), previously associated with the temporal dynamics of acute inflammation and resolution [17] (Fig. 4a, b, Supplementary Fig. 7). We found that during swarming, in addition to LTB_4, human neutrophils also produce large amounts of lipoxin A_4 (LXA_4), resolvin E3 (RvE3), prostaglandins D_2 (PGD_2) and E_2 (PGE_2) (Supplementary Table 2). Interestingly, there is almost a 20-fold increase in the production of LXA_4 at three hours, while RvE3 peaks early and remains nearly constant after one hour. The PGD_2 and PGE_2 prostaglandins have a peak in production in the first 30 minutes (2.5 ± 0.9 pg/mL) after the initiation of swarming, comparable to maximum LTB4 levels (4.4. ± 1.0 pg/mL), suggesting a complex interplay of signals and the presence of an equilibrium point or “eicosanoid switch” [18]. Using this microscale array of particle-clusters, we also identified neuroprotectin D1/protectin D1 (NPD1/PD1), which is also a chemical signal and member of the specialized pro-resolving mediators superfamily [19]. Although it was released from neutrophil swarms, we did not observe temporal changes in its levels during the growth of the swarms. We verified the role of LXA_4 as a stop signal during neutrophil swarming by pre-treating the neutrophils with LXA_4 before the swarming assay and by adding LXA_4 to the media during swarming. We observed significantly smaller swarms, that grow at significantly slower rates in the presence of LXA_4 compared to controls (Fig. 4c).

Protein mediators of human neutrophil swarming

We also investigated the release of protein mediators in the small volume above the array of synchronized neutrophil swarms. We employed multiplex quantitative ELISA and measured the concentrations of 440 cytokines, proteases, protease inhibitors, and soluble receptors in the supernatant, at 30, 60 and 180 minutes after the start of swarming (Supplementary Table 3). We identified ten proteins released at significantly higher levels by human neutrophils during swarming (Fig. 5a, Supplementary Tables 4 and 5). Among these, Galectin-3 is secreted at ~10 fold higher levels by swarming than non-swarming neutrophils, and ~100 fold higher than those released by non-activated controls. Additional support for the contribution of the ten swarm-specific molecular species to swarming dynamics is provided by the increase in their concentrations at 30, 60 and 180 minutes after the initiation of swarming (Fig. 5c). We also found 29 released proteins at distinct levels between activated neutrophils (swarming and non-swarming) and controls (Fig. 5b, Supplementary Tables 5 and 6). Several other proteins contribute to the activation and migration of other immune and non-immune cells. The levels of these proteins change over time, for example, we measured a 30 fold increase in peptidoglycan recognition proteins (PGRP-S) during swarming (Supplementary Fig. 8).

Altered swarming behavior of neutrophils from patients

We probed the swarming behavior of neutrophils from patients after trauma and found that they are recruited slower and give rise to smaller swarms compared to the neutrophils from healthy individuals. We isolated neutrophils from 16 blood samples collected from 8 trauma patients at 2–3 days interval (Supplementary Table 7). We found that the ability of neutrophils to form swarms is significantly reduced and the size of swarms for neutrophils from patients is smaller than neutrophils from healthy controls (Fig. 6a). In patients, the plateau swarm size was 645.8 ± 144.1 μm^2, 698.3 ± 212.8 μm^2, and 635.2 ± 191.9 μm^2 for trauma, autoimmune disease, and sepsis patients respectively. However, experimental controls run at the same conditions had a plateau size at 1373.2 ± 378.8 μm^2 (Fig. 6b). For patients recovering after trauma, the average size of the swarms was smaller in the early days after trauma and increased at later time points (Fig. 6c). Detailed observations of neutrophil dynamics during swarming showed a significant delay in the initiation of swarming after interaction with zymosan particle clusters (scouting phase) and slower growth - Fig. 6d). We also measured larger variations in the migration speed towards swarms for neutrophils from patients compared to controls (Supplementary Fig. 9).

Discussion

We employed arrays of thousands of clusters of zymosan particles to perform comprehensive studies of human neutrophil swarming. This microscale array enables comprehensive studies of human neutrophils and overcomes significant limitations of previous studies. For example, the study of neutrophil swarming in mouse and zebrafish models [1,2,16] lacks control over the target size and triggers the response of heterogeneous populations of leukocytes from which the molecular signals released by neutrophils cannot be dissected. A key feature of the microscale array is the ability to synchronize the swarming of thousands of neutrophils. In combination with the low volume of supernatant, this enables unprecedented sensitivity for measuring signaling molecules released at different stages during swarming. Moreover, the microscale array enables comparisons between neutrophils interacting with particles in swarming and non-swarming conditions, which share the activation by the same zymosan particles and are distinct from un-activated neutrophils. The precise control of the size of the zymosan-particle clusters is key for these controls and leverages the dependence of swarming on the size of the clusters and the arrangement of the particles. It also enabled us to quantify the traffic of neutrophils between swarms formed around targets that are heterogeneous in size, a situation that closely resembles the transient swarms observed during *in vivo* infections.[11] However, unlike typical infections, swarming around zymosan particles is likely triggered by the first neutrophils interacting with the target rather than soluble signals diffusing from the infection site. The first neutrophils arrive to the targets by chance during the loading of the devices and subsequent neutrophils are guided by mediators released from the first cells. In the presence of serum, an additional mediator for the early interactions between neutrophils and targets may be complement factors converted to chemoattractants in the presence of zymosan [20,21]. This potential mechanisms is dispensable however, as demonstrated by our experiments in which swarming occurs in serum free media. The mechanism of swarm initiation in our experiments also appears to be independent of cell or tissue damage [1,2,22] and does not require the presence of

monocytes [6]. The processes replicated on the microscale array of particle-clusters is thus relevant to neutrophil-pathogen encounters during infections.

One of the intriguing findings using the swarming array is that several mediators contribute to the robust swarming of human neutrophils. Among these, LTB_4 plays the dominant role during human neutrophil swarming, similar to the findings in mice from single gene knockouts. In addition to LTB4, we found that other mediators can also contribute to swarming, e.g. CXCL8 and complement factors, but only when the actions of LTB_4 are inhibited. The ability of neutrophils to produce CXCL8 is consistent with previously reports of LTB4 and CXCL8 production by neutrophils after interaction with zymosan particles [23,24], and the conversion of complement factors in plasma following incubation with zymosan [21]. In addition to these factors, we also identified ten swarming-specific proteins released during the early stages of swarming. Four of these (Galectin-3, Nidogen-1, CXCL7, and TSP-1) are known to enhance human neutrophil motility[25–28]. Several others are known to contribute to the activation of monocytes (CXCL7) [29], lymphocytes (PGRP-S) [30], and fibroblasts (PDGF-BB) [31], and endothelial cells (Galectin-3) [32]. Lipocalin-2, an iron sequestering protein that limits bacterial growth [33], and Galectin-3, an antimicrobial protein with activity against bacteria and fungi [32], interfere with microbial activities in the tissues and are produced in significantly higher amounts during swarming compared to phagocytosis controls. All mediators that are significantly higher during swarming display a monotonic concentration increase after the start of the swarm. One notable exception is complement activator Pentraxin-3 [34]. It is possible that Pentraxin-3 is degraded by the proteases released during swarming as a mechanism limiting inflammation. The balance between proteases and inhibitors e.g tissue inhibitor of matrix metalloproteinase (TIMP-1), which is released in large amount during swarming, appears to be important for the interaction between swarms and the local tissue environment, enabling the accumulation of more neutrophils, while at the same time limiting the potential damage to tissues [35]. Together, these signals coordinate not only the growth of neutrophil swarms, but the interactions with other immune and non-immune cells, to accomplish fast and robust responses that will protect healthy tissues from injuries and/or infectious aggressions.

In contrast to the large number of protein mediators that serve to enhance neutrophil accumulation during swarming, only two of the superfamily of resolution phase signals that stop neutrophil recruitment were identified during the development of the neutrophil swarms. These include lipoxin A_4 (LXA_4) and resolvin E3 (RvE3) [36], two very potent mediators of inflammation resolution [37]. Their role in controlling swarm size is new, consistent with their production during the plateau phase of swarming, and with reduced size and slower growth of the swarms in the presence of LXA_4. Although the recruitment role of PGD_2 for some leukocytes has been reported [38], this is the first evidence that human neutrophils produce PGD_2 during neutrophil swarming. Our findings are in agreement with experiments in which combinations of elevated levels of LTB_4 and PGD_2 are found in the airways, bronchoalveolar lavages (BALs), and exhaled breath condensates of asthma patients [39,40]. The same signals may be at play in patients in critical condition [41] and provide an explanation for our observations of the reduced size of swarms in this patient population. The deficit in swarming may also be due to inability of the neutrophils from patients to follow chemical gradients, to release chemical mediators to stimulate other cells to migrate,

or both. Some of the motility defects for neutrophils from patients in critical condition are already known[42], and more types of defects are likely to emerge from the detailed analysis of swarming using neutrophils from patients. Better understanding of the sources for swarming deficiencies will ultimately lead new treatments to enhance the ability of neutrophils to contain areas of tissue damage and infections and reduce the susceptibility for infections in patients during critical care [43].

Methods

Chemicals

Commercially available high molecular weight cationic copolymer of polyacrylamide and quaternized cationic monomer (ZETAG 8185, BASF, Florham Park, NJ, USA) was used as ink for PDMS microstamps. Fluorescent zymosan derived from *S. cerevisiae* was used as model, yeast-like target (Z2843, Life Technologies, Carlsbad, CA, USA). Zymosan particles were treated with an opsonizing reagent (Z2850, Life Technologies, Carlsbad, CA, USA) before use, following a protocol provided by the manufacturer. Glutaraldehyde, osmium tetraoxide, and 0.1 M sodium cacodylate were used for neutrophil fixation. U75302 and LY255283 (Catalog number: 70705 and 70715, Cayman Chemicals, Ann Arbor, MI, USA) were used as BLT1 and BLT2 receptor antagonists during LTB_4 production. LXA_4 (Catalog number: 90410, Cayman Chemicals, Ann Arbor, MI, USA) was used as an exogenous inhibitor for neutrophil migration. Human CXCR1 and CXCR2 antibodies (Catalog Number: MAB330 and MAB331, R&D Sytems, MN, USA) were used to block recognition of secreted IL-8 by activated neutrophils. We used heat-inactivated serum (System Biosciences, Mountain View, CA, USA) to test the influence of heat-labile C5a and C3a factors during neutrophil recruitment.

Microfabrication of the stamp

Device fabrication was performed using standard soft-lithography techniques on a four-inch wafer. Three layers of photoresist (SU-8, Michrochem, Newton, MA, USA) were spun onto a silicon wafer. The photoresist was exposed to UV light using a mask aligner (Neutronix Quintel), and the unexposed photoresist was developed away to yield multiple arrays of posts with heights of 15 μm, diameters of 10 or 20 μm, and spacing of 20, 40, 80, 100, or 200 μm. A 10:1 ratio of polydimethylsiloxane (PDMS) and its curing agent (SYLGARD 184 A/B, Dow Corning, Midland, MI, USA) was poured onto wafers and cured overnight at 65 °C. The PDMS layer was peeled off and the arrays of posts were punched out using an 8 mm biopsy punch (Harris Uni-Core, Ted Pella Inc, Redding, CA, USA) to create stamps.

To prepare the stamps for patterning, high molecular weight cationic FITC-ZETAG was used as ink. Stamps were placed face up, and 100 μL of ink was pipetted onto the PDMS micro post array. The stamps were then placed face down into a reservoir dish containing 1 mL of ink and allowed to incubate for at least 10 minutes. Stamps were then pressed onto a glass slide to remove excess ink, before being pressed with 3.7 g weights onto a plasma treated glass slide (Fisherbrand Double Frosted Microscope Slides, Fisher Scientific, Waltham, MA, USA). Stamps were spaced into wells using 8-well imaging spacers. After 5 minutes, weights and stamps were removed and allowed to dry to yield patterned ZETAG. For each

patterned slide, we cut 8 mm wells using a biopsy punch in flat, 2 mm thick pieces of PDMS. The wells were sealed to the glass using a double-stick spacer (Secure-Seal, Grace Bio-Labs, Bend, OR, USA).

Fluorescent zymosan particle clusters were used as targets for neutrophils swarms. A solution of 0.5 mg/mL zymosan particles in ultra-pure water was pipetted onto the patterned ink and was allowed to adhere to the ink by electrostatic interactions. Excess zymosan was then washed away by flushing thoroughly with deionized water, and samples were stored at 4°C.

Neutrophil Isolation

Fresh human blood samples from healthy volunteers, aged 18 years and older, were purchased from Research Blood Components (Allston, MA, USA). All blood specimens from patients were obtained with informed consent according to an institutional review board (IRB) approved protocol at the Massachusetts General Hospital. Peripheral blood was drawn into heparinized-tubes (Vacutainer; Becton Dickinson, Woburn, MA, USA) and human neutrophils were isolated within 2 hours after blood collection using EasySep Human Neutrophil Enrichment Kits by following manufacturer instructions (STEMCELL Technologies, Vancouver, Canada). After isolation, neutrophils were washed using cell culture medium, and the nuclei were stained with Hoechst 33342 trihydrochloride dye (Life Technologies, Woburn, MA, USA). Stained neutrophils were then resuspended in medium at a density of 7.5×10^5 cells per mL. Two hundred microliters of cell suspension were then pipetted into each well containing the array of zymosan particle clusters and sealed with a 12 mm diameter coverslip. The purity of the neutrophils was estimated by flow cytometry (using anti-CD66b fluorescent antibodies and Hoechst nuclear stain). Less than 0.1% of the isolated neutrophils had platelets attached to their surface (quantified using anti-CD61 fluorescent antibodies - Supplementary Fig. 10.).

Neutrophil Inhibition

LY255283 was dissolved in ethanol. LY255283, U75302, and LXA_4 solutions were vacuum dried for 5 min. Each compound was re-suspended in cell culture media at a concentration of 20 μM for LY255283 and U75302 and 5 μM for LXA_4. For BLT1&2 inhibition, isolated neutrophils were re-suspended at 1/1 volume ratio of LY255283 and U75302 and incubated for 10 min before to add the neutrophils on the swarming assay. For testing the effect of LXA_4 on neutrophil migration during swarming, neutrophils were re-suspended on 5 μM LXA_4 and added to the assay immediately.

Neutrophil Imaging

After neutrophil loading, cell behavior was recorded using time-lapse imaging at 10x magnification in a fully automatic Nikon TiE microscope (Micro Device Instruments, Avon, MA, USA) with a heated incubator to 37°C and 5 % CO_2. The maximum time resolution of acquisition was 0.2 frames per second to achieve accurate neutrophil tracking.

Swarm Size Measurement

Swarm size and size changes over time were estimated using the surface segmentation module in Imaris. The cell-occupied area was measured from the Hoechst labeled neutrophils using a 2 pixel smoothing filter with background subtraction and automatic thresholding. Individual cells not contacting the particle cluster were excluded with a minimum area filter of 5 μm, and an automatic minimum intensity filter in the particle cluster (zymosan) TxRed channel. This allowed us to measure the area over time of the remaining single surface object, which corresponded to cells within the swarm contiguous with the particle cluster.

Single Neutrophil Tracking

Cells were tracked using Imaris spot detection and tracking (Bitplane). Cells were detected with a spot radius of 5 μm (to match the approximate cell size), with background subtraction enabled and with a minimum quality of 1.7. Tracking was performed using an autoregressive motion model, with a maximum displacement of 5 μm and a maximum gap length of 3 frames. Tracks were eliminated which did not have a duration spanning at least ½ of the dataset. Cell tracks were then exported for analysis in Matlab.

Chemotaxis Analysis

The instantaneous chemotactic index (CI) at time t was then calculated as: $CI(t)=\frac{-R'(t)}{X'(t)}$

where: $R'(t)=\frac{\partial}{\partial t}\|x-z\|$ is the rate of change of the distance between the cell's position x and the zymosan particle cluster position z. Prior to chemotaxis, analysis the cell track positions x were smoothed by spline fitting (MATLAB function *spaps*), with a tolerance selected for each track such that 95% of the spline fit residuals were ≤ 2.5 μm, the approximate average cellular radius. Clusters of zymosan particles were segmented by Otsu thresholding followed by selection of the largest connected component, and z was set to be the centroid of this object. Cellular migration speed (spline smoothed) is calculated as:

$X'(t)=\|\frac{\partial x}{\partial t}\|$.

Chemotactic index maps were created by averaging the CI of all cells within the specified distance and time bins. The maximum distance for these maps was set based on the minimum distance from the particle cluster centroid z to the image border, and thus the radius of the largest circle centered on the particle cluster that was completely contained within the image. Because the distance to the particle cluster is approximated by its centroid, the true distance will differ depending on the shape and radius of this particle cluster. To minimize the effect of this error, the minimum distance for the CI maps was set to:

$Z_{\min}=4\sqrt{\frac{a}{\pi}}$ where a is the area of the zymosan particle cluster. This distance cutoff corresponds to the radius where the distance error would exceed 50% for a disk shaped particle cluster with the same area.

Diffusion Modeling

Chemoattractant diffusion properties (including diffusion coefficients D) were estimated by simultaneously fitting both a diffusion model and a cellular response model to the measured chemotactic index maps. We modeled the concentration c_i produced by a single instantaneous release of chemoattractant at time t_i as:

$$c_i(r,t)=\frac{2m_i}{(4\pi D(t-t_i))^{3/2}}e^{\frac{-r^2}{4D(t-t_i)}}$$

where r is the distance from the particle cluster, t is time, m_i is the mass of chemoattractant released, and D is the diffusion coefficient. The factor of 2 accounts for the fact that the domain into which the chemoattractant is being released is bounded on one side by the coverslip to which the cells and particle cluster are adhered (using the principle of superposition). Releases of finite duration were modeled by the superposition of these instantaneous releases. For example, the concentration C(r, t) resulting from a continuous release starting at time T_r was modeled as:

$$C(r,t)=\sum_i c_i(r,t)$$

$$m_i=\begin{cases} 0, & t_i<T_r \\ M, & t_i \geq T_r \end{cases}$$

with the vector t of individual release times t_i set to

$$t=\{T_r, T_r+\Delta, T_r+2\Delta, \ldots, T_e\}$$

where T_e is the end of the image series and where Δ was set to 1 second (1/5th of the imaging interval). This diffusion model was then linked to cellular chemotaxis via a cellular response model:

$$CI_p(r,t)=p_b+\frac{p_m+p_b}{1+e^{-s(C(r,t)-C_0)}}$$

where CI_p(r, t) is the predicted mean chemotactic index at a given radius and time, with p_b the basal chemotactic index (in the absence of chemoattractant), p_m is the maximum CI, s is the slope of the cellular response to chemoattractant and C_0 is the concentration at which the cellular CI response is half of its maximum (.5p_m). All model free parameters were then estimated by least squares minimization:

$$\underset{D,M,T_r,p_m,p_b,s,C_0}{\arg\min}\sum_{r,t}(\mathrm{CI}(r,t)-CI_p(r,t))^2$$

As this objective function is non-convex, we used parallelized multi-start nonlinear least squares minimization (MATLAB MultiStart). We performed a parameter sweep of the number of starting points on a subset of the data to confirm that above 2000 initializations the resulting model fits and parameter estimates were stable.

Electron Microscopy

Neutrophil swarms were chemically fixed with 2 % glutaraldehyde in 0.1 M sodium cacodylate for 2 h. Then, samples were gradually dehydrated in different percentages of ethanol (50 %, 70 %, 80 %, 95 %, and 100 % V/V) for 15 min each. Samples were transferred to a CO_2 critical point drier Autosamdri 931 (Tousimins, Rockville, MD, USA). Dried samples were sputtered with a Platinum/Palladium target at a rate of 10 Å/min for a total thickness of 10 nm. Scanning electron microscopy (SEM) was conducted with a Supra FV500 (Zeiss, Peabody, MA, USA). Samples were imaged at different magnifications using an accelerating voltage of 3 kV.

Lipid Mediator Metabololipidomics of Swarm Supernatant

Four different healthy donors were tested to compare temporal lipid mediator profiles. To minimize artifacts of neutrophil activation cells were isolated and not stained. After neutrophil isolation, cells were suspended in IMDM media without phenol red and supplemented with 0.4 % human serum albumin (HSA, Sigma-Aldrich, Saint Louis, MO, USA). The supernatant of different wells was collected at different time points (0, 0.5, 1, and 3 h), flash frozen at −80°C, and stored. Supernatants were placed in 2 volumes of ice-cold methanol and kept at −20°C to allow for protein precipitation, and lipid mediators were extracted using solid-phase extraction as in [44]. Briefly, before sample extraction, deuterated internal standards (d_4-PGE_2, d_5-LXA_4, d_4-RvD2, d_4-LTB_4, d_5-LTC_4 and d_8-5S-HETE) representing regions of interest in the chromatographic analysis (500 pg each) were added to facilitate quantification. Extracted samples were analyzed by an LC-MS-MS system, Qtrap 6500 (AB Sciex) equipped with a Shimadzu SIL-20AC autoinjector and LC-20AD binary pump (Shimadzu Corp.). An Agilent Eclipse Plus C18 column (100×4.6mm×1.8μm) was used with a gradient of methanol/water/acetic acid of 55:45:0.01 (vol:vol:vol) that was ramped to 85:15:0.01 (vol:vol:vol) over 10 min and then to 98:2:0.01 (vol:vol:vol) for the next 8 min. This was subsequently maintained at 98:2:0.01 (vol:vol:vol) for 2 min. The flow rate was maintained at 0.4ml/min. To monitor and quantify the levels of lipid mediators, a multiple reaction monitoring (MRM) method was developed with signature ion fragments (m/z) for each molecule monitoring the parent ion (Q1) and a characteristic daughter ion (Q3). Identification was conducted using published criteria for each molecule where a minimum of 6 diagnostic ions were employed [44]. Calibration curves were determined using a mixture of synthetic lipid mediators standards obtained via total organic synthesis. Linear calibration curve for each compound was obtained with r^2 values ranging from 0.98 to 0.99. The detection limit was ~0.1 pg for each lipid mediator. Quantification was carried out as detailed in ref. [44].

Released Proteins Analysis

The analysis for the presence of cytokines and chemokines released during swarming was conducted at RayBiotech (Norcross, GA, USA) using a high throughput sandwich ELISA-

based quantitative array platform Q9000. We tested neutrophil swarming supernatants against over 400 proteins. Each protein was tested in quadruplicate. For protein quantification, the array had each single protein as a control and at known concentrations to generate standard curves for each protein. By comparing signals from the samples to the individual standard curves, the protein concentrations in the samples were determined.

Statistical Analysis

Differences in secreted proteins levels between swarms and resting neutrophils were evaluated using the software package JMP (Version 11). The Shapiro-Wilk test was used to ensure the data were normally distributed, and homogeneity of variance was tested using Levene's test. ANOVA Randomized Complete Block Design (RCB) was then performed as appropriate. Where statistically significant differences were found in the ANOVA, the Tukey-Kramer HSD test was carried out to find out which groups differed. When the assumptions (normality and homoscedasticity) were not valid, ANOVA on the transformed data or Kruskal-Wallis test was conducted. Differences were deemed statistically significant for p values of less than 0.05.

Supplementary Material

Refer to Web version on PubMed Central for supplementary material.

Acknowledgments

We thank Mr. Bashar Hamza and Dr. Joseph M. Martel of the BioMEMS Resource Center for help with microfabrication and stimulating discussions. This work was supported by a grant from the National Institute of General Medical Sciences (GM092804) and funding from the HMS Tools and Technology Fund. Microfabrication was conducted at the BioMEMS Resource Center at Massachusetts General Hospital, supported by a grant from the National Institute of Biomedical Imaging and Bioengineering (EB002503). Work in the CNS labs was supported by the National Institutes of Health (GM095467 and GM38765).

References

1. Ng LG, et al. Visualizing the neutrophil response to sterile tissue injury in mouse dermis reveals a three-phase cascade of events. The Journal of investigative dermatology. 2011; 131:2058–2068. [PubMed: 21697893]
2. Lammermann T, et al. Neutrophil swarms require LTB4 and integrins at sites of cell death in vivo. Nature. 2013; 498:371–375. [PubMed: 23708969]
3. Afonso PV, et al. LTB4 is a signal-relay molecule during neutrophil chemotaxis. Dev Cell. 2012; 22:1079–1091. [PubMed: 22542839]
4. Kienle K, Lammermann T. Neutrophil swarming: an essential process of the neutrophil tissue response. Immunol Rev. 2016; 273:76–93. [PubMed: 27558329]
5. Jones CN, et al. Microfluidic assay for precise measurements of mouse, rat, and human neutrophil chemotaxis in whole-blood droplets. Journal of leukocyte biology. 2016; 100:241–247. [PubMed: 26819316]
6. Malawista SE, de Boisfleury Chevance A, van Damme J, Serhan CN. Tonic inhibition of chemotaxis in human plasma. Proceedings of the National Academy of Sciences of the United States of America. 2008; 105:17949–17954. [PubMed: 18997012]
7. Lammermann T. In the eye of the neutrophil swarm-navigation signals that bring neutrophils together in inflamed and infected tissues. Journal of leukocyte biology. 2016; 100:55–63. [PubMed: 26416718]

8. Liese J, Rooijakkers SH, van Strijp JA, Novick RP, Dustin ML. Intravital two-photon microscopy of host-pathogen interactions in a mouse model of Staphylococcus aureus skin abscess formation. Cell Microbiol. 2013; 15:891–909. [PubMed: 23217115]
9. Kamenyeva O, et al. Neutrophil recruitment to lymph nodes limits local humoral response to Staphylococcus aureus. PLoS Pathog. 2015; 11:e1004827. [PubMed: 25884622]
10. Kreisel D, et al. In vivo two-photon imaging reveals monocyte-dependent neutrophil extravasation during pulmonary inflammation. Proceedings of the National Academy of Sciences of the United States of America. 2010; 107:18073–18078. [PubMed: 20923880]
11. Chtanova T, et al. Dynamics of neutrophil migration in lymph nodes during infection. Immunity. 2008; 29:487–496. [PubMed: 18718768]
12. Bruns S, et al. Production of extracellular traps against Aspergillus fumigatus in vitro and in infected lung tissue is dependent on invading neutrophils and influenced by hydrophobin RodA. PLoS Pathog. 2010; 6:e1000873. [PubMed: 20442864]
13. Jones CN, et al. Human Neutrophils Are Primed by Chemoattractant Gradients for Blocking the Growth of Aspergillus fumigatus. The Journal of infectious diseases. 2016; 213:465–475. [PubMed: 26272935]
14. Leliefeld PH, Wessels CM, Leenen LP, Koenderman L, Pillay J. The role of neutrophils in immune dysfunction during severe inflammation. Crit Care. 2016; 20:73. [PubMed: 27005275]
15. Malawista SE, de Boisfleury AC, Naccache PH. Inflammatory gout: observations over a half-century. FASEB journal : official publication of the Federation of American Societies for Experimental Biology. 2011; 25:4073–4078. [PubMed: 22131362]
16. Boneschansker L, Yan J, Wong E, Briscoe DM, Irimia D. Microfluidic platform for the quantitative analysis of leukocyte migration signatures. Nature communications. 2014; 5:4787.
17. Serhan CN. Novel lipid mediators and resolution mechanisms in acute inflammation: to resolve or not? Am J Pathol. 2010; 177:1576–1591. [PubMed: 20813960]
18. Levy BD, Clish CB, Schmidt B, Gronert K, Serhan CN. Lipid mediator class switching during acute inflammation: signals in resolution. Nature immunology. 2001; 2:612–619. [PubMed: 11429545]
19. Serhan CN, et al. Anti-inflammatory actions of neuroprotectin D1/protectin D1 and its natural stereoisomers: assignments of dihydroxy-containing docosatrienes. Journal of immunology. 2006; 176:1848–1859.
20. Hammerschmidt DE, Bowers TK, Lammi-Keefe CJ, Jacob HS, Craddock PR. Granulocyte aggregometry: a sensitive technique for the detection of C5a and complement activation. Blood. 1980; 55:898–902. [PubMed: 6991024]
21. Wagner JL, Hugli TE. Radioimmunoassay for anaphylatoxins: a sensitive method for determining complement activation products in biological fluids. Anal Biochem. 1984; 136:75–88. [PubMed: 6711816]
22. Harvie EA, Green JM, Neely MN, Huttenlocher A. Innate immune response to Streptococcus iniae infection in zebrafish larvae. Infection and immunity. 2013; 81:110–121. [PubMed: 23090960]
23. Bazzoni F, et al. Phagocytosing neutrophils produce and release high amounts of the neutrophil-activating peptide 1/interleukin 8. The Journal of experimental medicine. 1991; 173:771–774. [PubMed: 1997655]
24. Guerrero AT, et al. Involvement of LTB4 in zymosan-induced joint nociception in mice: participation of neutrophils and PGE2. Journal of leukocyte biology. 2008; 83:122–130. [PubMed: 17913976]
25. Bhaumik P, St-Pierre G, Milot V, St-Pierre C, Sato S. Galectin-3 facilitates neutrophil recruitment as an innate immune response to a parasitic protozoa cutaneous infection. Journal of immunology. 2013; 190:630–640.
26. Lopez-Dee Z, Pidcock K, Gutierrez LS. Thrombospondin-1: multiple paths to inflammation. Mediators Inflamm. 2011; 2011:296069. [PubMed: 21765615]
27. Schenk BI, Petersen F, Flad HD, Brandt E. Platelet-derived chemokines CXC chemokine ligand (CXCL)7, connective tissue-activating peptide III, and CXCL4 differentially affect and cross-regulate neutrophil adhesion and transendothelial migration. Journal of immunology. 2002; 169:2602–2610.

28. Senior RM, Gresham HD, Griffin GL, Brown EJ, Chung AE. Entactin stimulates neutrophil adhesion and chemotaxis through interactions between its Arg-Gly-Asp (RGD) domain and the leukocyte response integrin. The Journal of clinical investigation. 1992; 90:2251–2257. [PubMed: 1469085]
29. Baltus T, et al. Differential and additive effects of platelet-derived chemokines on monocyte arrest on inflamed endothelium under flow conditions. Journal of leukocyte biology. 2005; 78:435–441. [PubMed: 15899984]
30. Dziarski R, Platt KA, Gelius E, Steiner H, Gupta D. Defect in neutrophil killing and increased susceptibility to infection with nonpathogenic gram-positive bacteria in peptidoglycan recognition protein-S (PGRP-S)-deficient mice. Blood. 2003; 102:689–697. [PubMed: 12649138]
31. Bornfeldt KE, et al. Platelet-derived growth factor. Distinct signal transduction pathways associated with migration versus proliferation. Annals of the New York Academy of Sciences. 1995; 766:416–430. [PubMed: 7486687]
32. Markowska AI, Liu FT, Panjwani N. Galectin-3 is an important mediator of VEGF- and bFGF-mediated angiogenic response. The Journal of experimental medicine. 2010; 207:1981–1993. [PubMed: 20713592]
33. Yang J, et al. An iron delivery pathway mediated by a lipocalin. Mol Cell. 2002; 10:1045–1056. [PubMed: 12453413]
34. Garlanda C, et al. Non-redundant role of the long pentraxin PTX3 in anti-fungal innate immune response. Nature. 2002; 420:182–186. [PubMed: 12432394]
35. Iyer RP, Patterson NL, Fields GB, Lindsey ML. The history of matrix metalloproteinases: milestones, myths, and misperceptions. Am J Physiol Heart Circ Physiol. 2012; 303:H919–930. [PubMed: 22904159]
36. Arita M, et al. Metabolic inactivation of resolvin E1 and stabilization of its anti-inflammatory actions. The Journal of biological chemistry. 2006; 281:22847–22854. [PubMed: 16757471]
37. Serhan CN. Pro-resolving lipid mediators are leads for resolution physiology. Nature. 2014; 510:92–101. [PubMed: 24899309]
38. Murata T, et al. Anti-inflammatory role of PGD2 in acute lung inflammation and therapeutic application of its signal enhancement. Proceedings of the National Academy of Sciences of the United States of America. 2013; 110:5205–5210. [PubMed: 23479612]
39. Crea AE, Nakhosteen JA, Lee TH. Mediator concentrations in bronchoalveolar lavage fluid of patients with mild asymptomatic bronchial asthma. Eur Respir J. 1992; 5:190–195. [PubMed: 1348480]
40. Montuschi P, Barnes PJ. Exhaled leukotrienes and prostaglandins in asthma. J Allergy Clin Immunol. 2002; 109:615–620. [PubMed: 11941309]
41. Dalli J, et al. Human Sepsis Eicosanoid and Proresolving Lipid Mediator Temporal Profiles: Correlations With Survival and Clinical Outcomes. Critical care medicine. 2017; 45:58–68. [PubMed: 27632672]
42. Jones CN, et al. Spontaneous Neutrophil Migration Patterns during Sepsis after Major Burns. PloS one. 2014; 9:e114509. [PubMed: 25489947]
43. Vincent JL. Nosocomial infections in adult intensive-care units. Lancet. 2003; 361:2068–2077. [PubMed: 12814731]
44. Colas RA, Shinohara M, Dalli J, Chiang N, Serhan CN. Identification and signature profiles for pro-resolving and inflammatory lipid mediators in human tissue. Am J Physiol Cell Physiol. 2014; 307:C39–54. [PubMed: 24696140]
45. Reátegui, E., et al. Dataset for Microscale arrays for the profiling of start and stop signals coordinating human-neutrophil swarming; figshare. 2017. p. 5024567http://dx.doi.org/10.6084/m9.figshare

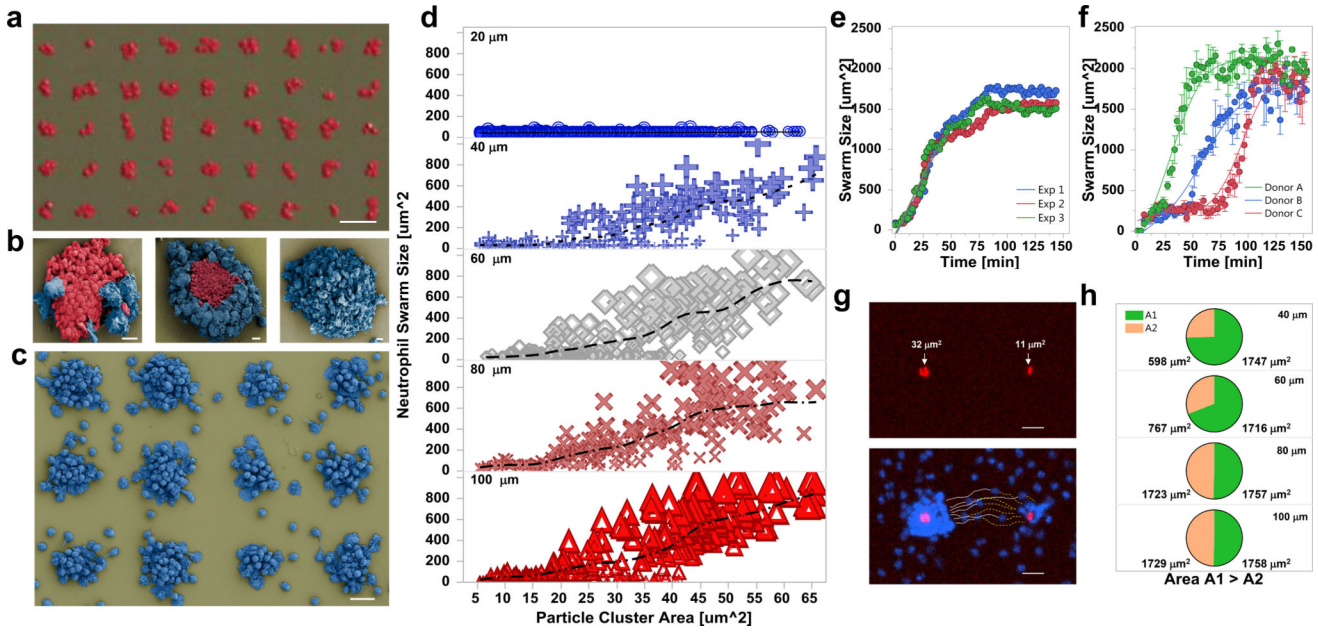

Figure 1. Human neutrophil swarming on large scale zymosan particle arrays

(a) Scanning electron micrograph (SEM) image of zymosan particle clusters patterned by electrostatic physisorption on 10 µm stamped ZETAG spots (scale bar: 20 µm). **(b)** SEM images of neutrophils in blue and zymosan particles in red at different stages of swarming. Early neutrophil scouting (left), neutrophil recruitment (center), neutrophil swarm completely covering zymosan particle clusters (right, images are at different magnifications, scale bar 5 µm for all panels). **(c)** An array of neutrophil swarms generated in the microfluidic assay at 60 min. Particle cluster targets are covered by neutrophils (blue), while other neutrophils are activated and migrating towards the swarms (scale bar: 20 µm). **(d)** Swarming depends on size of particle cluster and spacing between clusters. Particle cluster area represents the projection of each aggregate of zymosan particles. Cluster spacing is defined as the distance between adjacent clusters. Swarms form on particle clusters that have an area larger than 17 μm^2 and are spaced further than 20 µm. Swarms have sizes significantly larger than the particle cluster area. Representative experiment of N = 10. **(e)** Swarming size and dynamics are reproducible. Neutrophil samples from the same donor display similar swarming dynamics on clusters of comparable area in three separate experiments (N = 3, technical replicates). **(f)** Neutrophils from different healthy donors form swarms that display distinct temporal dynamics and reach distinct sizes. The variability between donors is larger than the differences measured in samples from the same donor. Each donor has been measured in three separate experiments (N = 3). Error bars represent standard deviations for these measurements. **(g)** Neutrophils (blue) traffic from the smaller to the larger zymosan cluster (red), contributing to the growth of larger swarms around the larger targets. The trajectories of the neutrophils joining the larger swarm to the left, on top of a large particle cluster are represented as solid white lines, while those leaving the smaller swarm to the right, formed on top of a small particle cluster are represented as dashed yellow tracks. (Scale bar: 15 µm). **(h)** When zymosan clusters of different size are closer than ~60 µm, neutrophils traffic from the smaller to the larger target, producing larger swarms around the larger targets. The relative size of the swarms for various distances

between targets is indicated in the pie charts, the absolute size is presented in numbers next to the charts. The larger clusters (A1) have areas between 50 and 60 μm^2 while the smaller clusters (A2) have areas between 35 and 45 μm^2. (N = 10 experiments, N = 100 adjacent swarms).

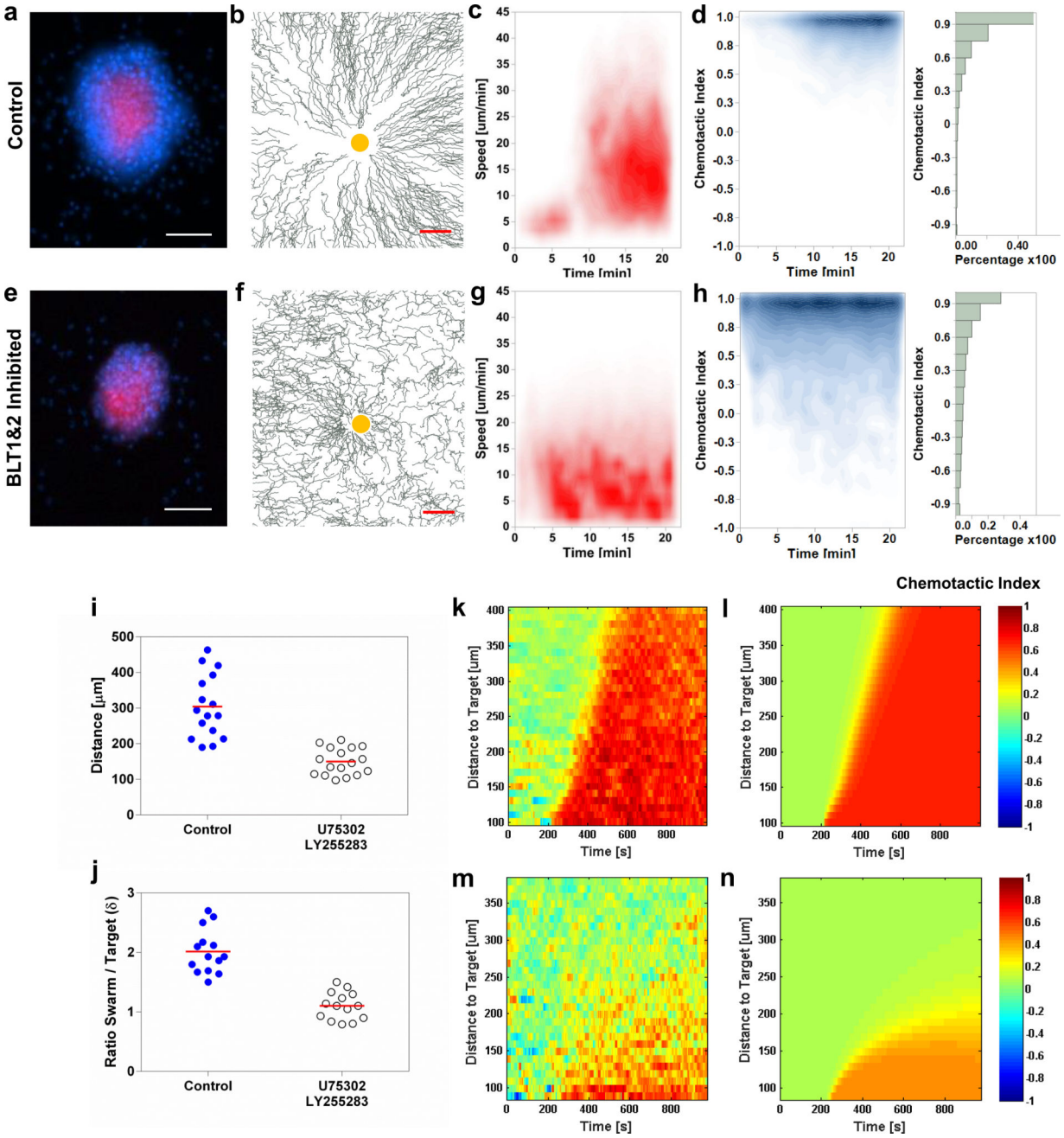

Figure 2. The migration of neutrophils towards swarms is altered in the presence of BLT1 and BLT2 antagonists

a–d. Characterization of neutrophil swarming in control experiments. **(a)** Neutrophils (blue) from healthy donors form large swarms around zymosan particle clusters (red) at 60 min (scale bar 100 μm). **(b)** Moving neutrophils display radial trajectories, centered on the particle cluster (scale bar 100 μm). **(c)** The speed of migration increases significantly at the end of the scouting phase and remains high during the accelerated growth phase of swarming (density plot of instantaneous migration speed for individual neutrophils). **(d)** The chemotactic index towards the particle clusters remains high over time, in agreement with

the qualitative aspects of the migration tracks (density plot of the instantaneous chemotactic index for individual neutrophils). A histogram of the distribution of chemotaxis indexes for the duration of the experiment. Panels a-d show representative experiments of N = 16. **e–h**. Characterization of neutrophil swarming in the presence of BLT1 and BLT2 receptors antagonists. **(e)** Neutrophils from the same healthy donors form smaller swarms in the presence of BLT1 and BLT2 receptors antagonists (60 min, scale bar: 100 μm). **(f)** Neutrophil migration patterns are more convoluted in the presence of BLT1 and BLT2 receptors antagonists (scale bar:100 μm). **(g)** The speed of migration is reduced and stable over time in the presence of BLT1 and BLT2 receptors antagonists. **(h)** The directionality of migration decreases and migrations away from the particle clusters become apparent (bi-directional migration pattern) in the presence of BLT1 and BLT2 receptors antagonists. A histogram of the distribution of chemotaxis indexes for the duration of the experiment shows a more shallow distribution compared to the controls. Panels e-h show representative experiments of N = 14. **(i)** Neutrophils are recruited from an area around the particle clusters, which has a radius that is ~50% shorter in the presence of receptor antagonists compared to controls (N = 16). The recruitment radius was measured as the maximum distance at which at least one neutrophil was recruited towards the target. We only considered the neutrophils that migrated persistently along the radial direction, towards the zymosan targets. Each dot represents a separate experiment for which at least 100 neutrophils were tracked towards the zymosan targets. **(j)** The ratio between the area of the swarm and the area of the particle cluster decreases in the presence of BLT1 and BLT2 antagonists compared to controls (N = 14). Red bars, mean (i–j). **k–n**. Biophysical model results and comparison to experimental data are consistent with the switch from a low molecular weight to a high molecular weight chemoattractant directing the neutrophils towards the swarm. (**k**) and (**m**) represent the experimental results for the control and antagonist conditions, showing that neutrophils are recruited from progressively larger areas around the particle clusters. (**l**) and (**n**) show the simulation results for fast and slow diffusing chemoattractants (1.2 and 0.6×10^{-10} m^2/s, respectively), produced at the location of the swarm, and released at comparable rates. The different colors on the graphs represent the chemotactic index, coded as detailed in the color bars to the right. On the color coded bar, 1 represents accurate radial migration towards the swarm, and −1 radial migration away from the swarm. The model provides support for the presence of at least one additional chemoattractant besides LTB_4 directing the migration of neutrophils towards swarms. Panels k-m show representative experiments of N = 5.

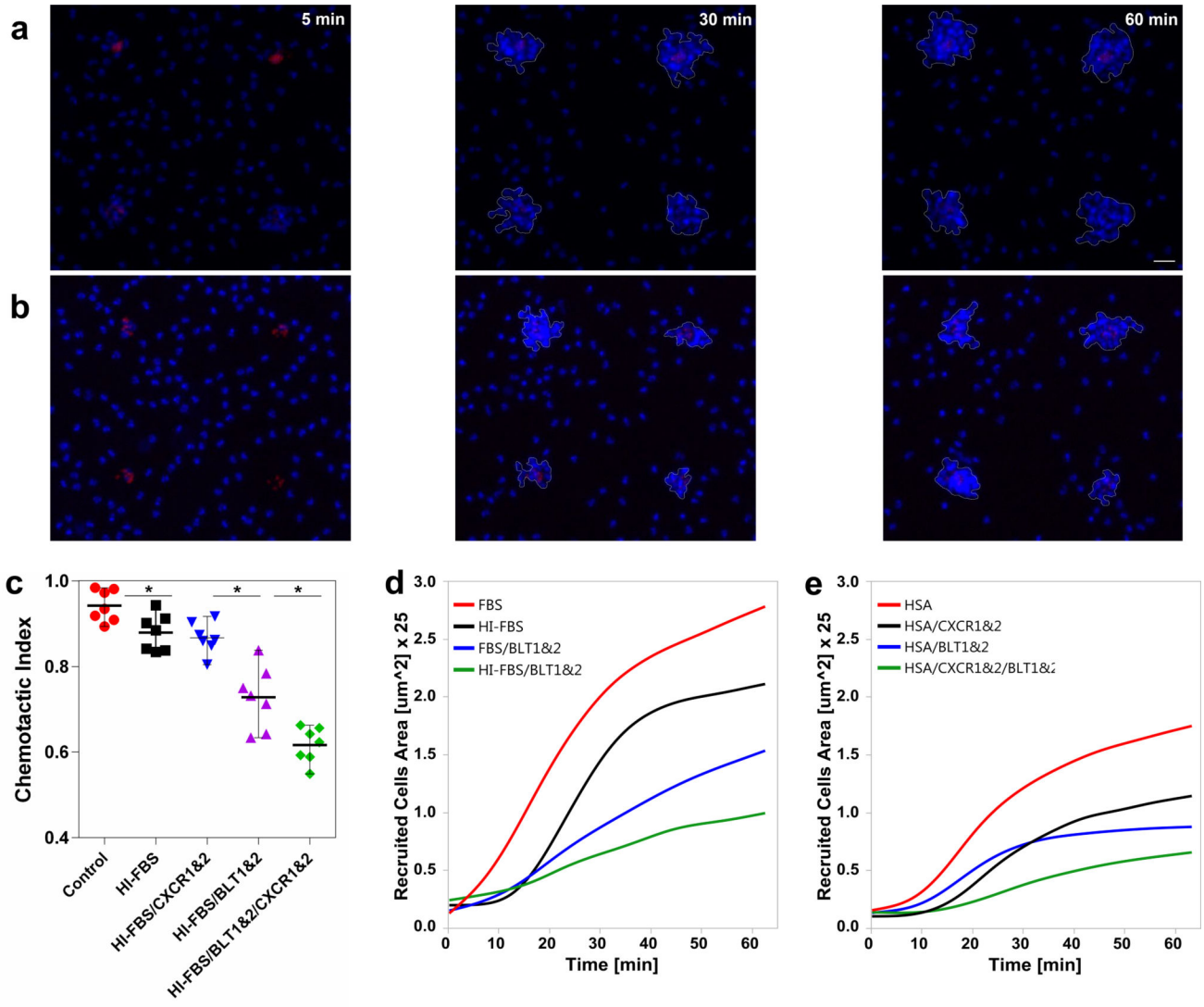

Figure 3. Evaluation of soluble factors guiding neutrophil migration during swarming

(a) In control conditions, swarms of neutrophils (blue) around patterned zymosan particle clusters (red) are observed at 5, 30 and 60 minutes. The contour of the swarms is emphasized by dashed white lines (scale bar: 20 μm; Representative experiment of N = 5). **(b)** Swarms grow slower and reach a smaller size in the presence of BLT1, BLT2, CXCR1 and CXCR2 receptor antagonists. (scale bar: 20 μm; Representative experiment of N = 5) **(c)** Changes in the chemotactic index (CI) during neutrophil swarming at various conditions of soluble factor inhibition. Control vs. Heat-inactivated serum (HI, $p < 0.05$), HI vs. CXCR1 and CXCR2 antagonists ($p > 0.05$), CXCR1 and CXCR2 antagonists vs. BLT1 and BLT2 antagonists ($p < 0.05$), BLT1 and BLT2 antagonists vs. CXCR1, CXCR2, BLT1 and BLT2 antagonists ($p < 0.05$). Error bars represent minimum and maximum value of the experimental group (*$p < 0.05$). **(d)** Comparison of the effect of heat-inactivated serum and BLT1 and BLT2 antagonists on the recruitment of neutrophils during swarming. (e) Inhibition of BLT1 and BLT2 and CXCR1 and CXCR2 for LTB4 and CXCL8

chemoattractants showed slower growth of swarms. Figures **d–e** show representative experiments of N = 5.

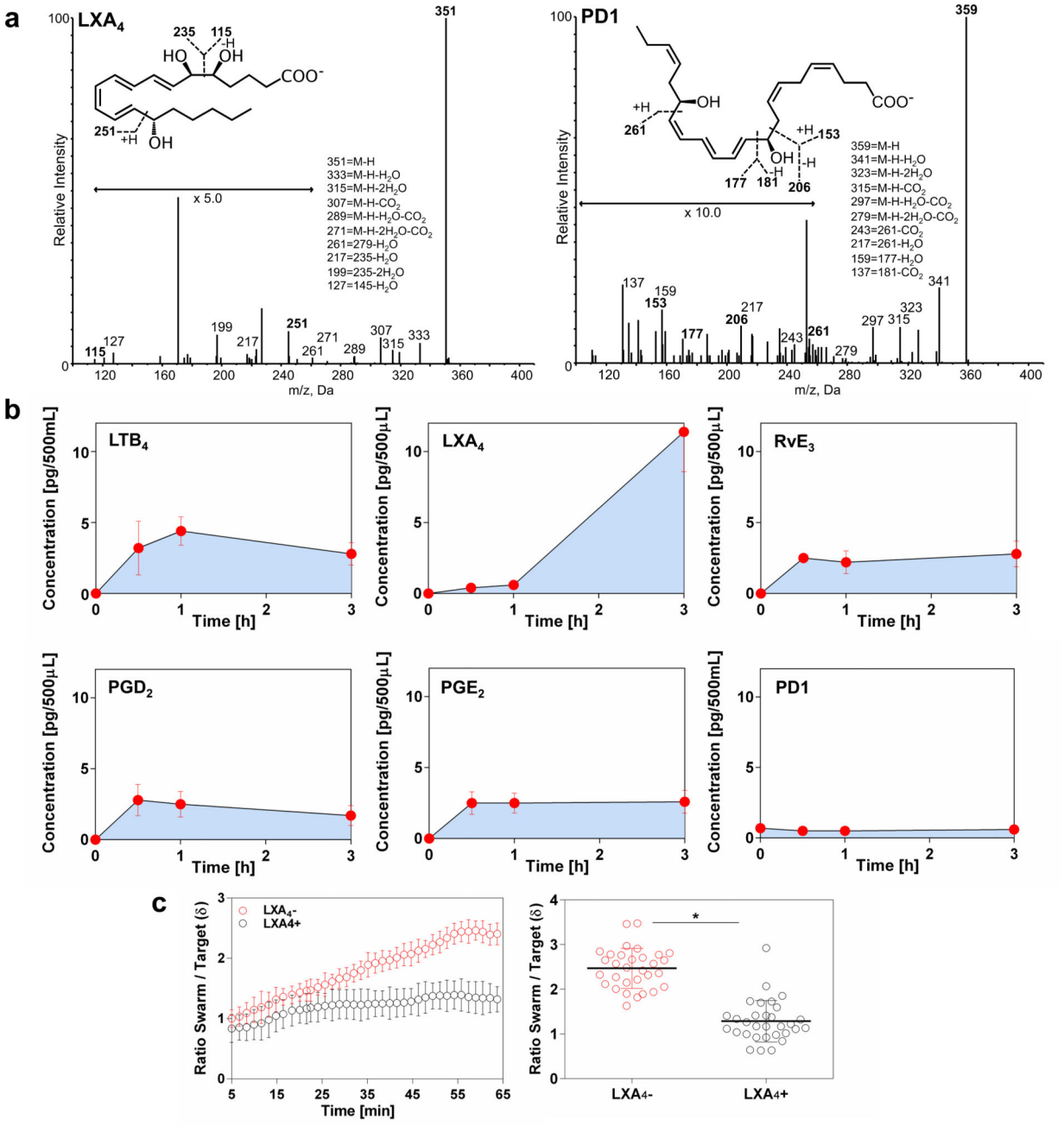

Figure 4. Lipid mediators released by human neutrophils during swarming

(a) Inflammation-initiating and pro-resolving lipid mediators released during human neutrophil swarming. Reference MS-MS fragmentation spectra employed for identification of PD1 and LXA_4 (N = 4 donors, n = 1850 swarms). **(b)** Transient profiles of inflammation mediators LTB4, PGD_2, and PGE_2, and resolution mediators LXA4, RvE3, and PD1, released during neutrophil swarming show different temporal dynamics. **c)** Characterization of neutrophil migration in the presence of exogenous LXA_4. [5 µM]. The recruitment profiles over time are slower in the presence of LXA4 compared to the control sample and

result in swarms with lower ratio of swarm to target size (δ_{Ratio}). Error bars represent standard error of the mean (* $p < 0.05$, N = 3 experiments).

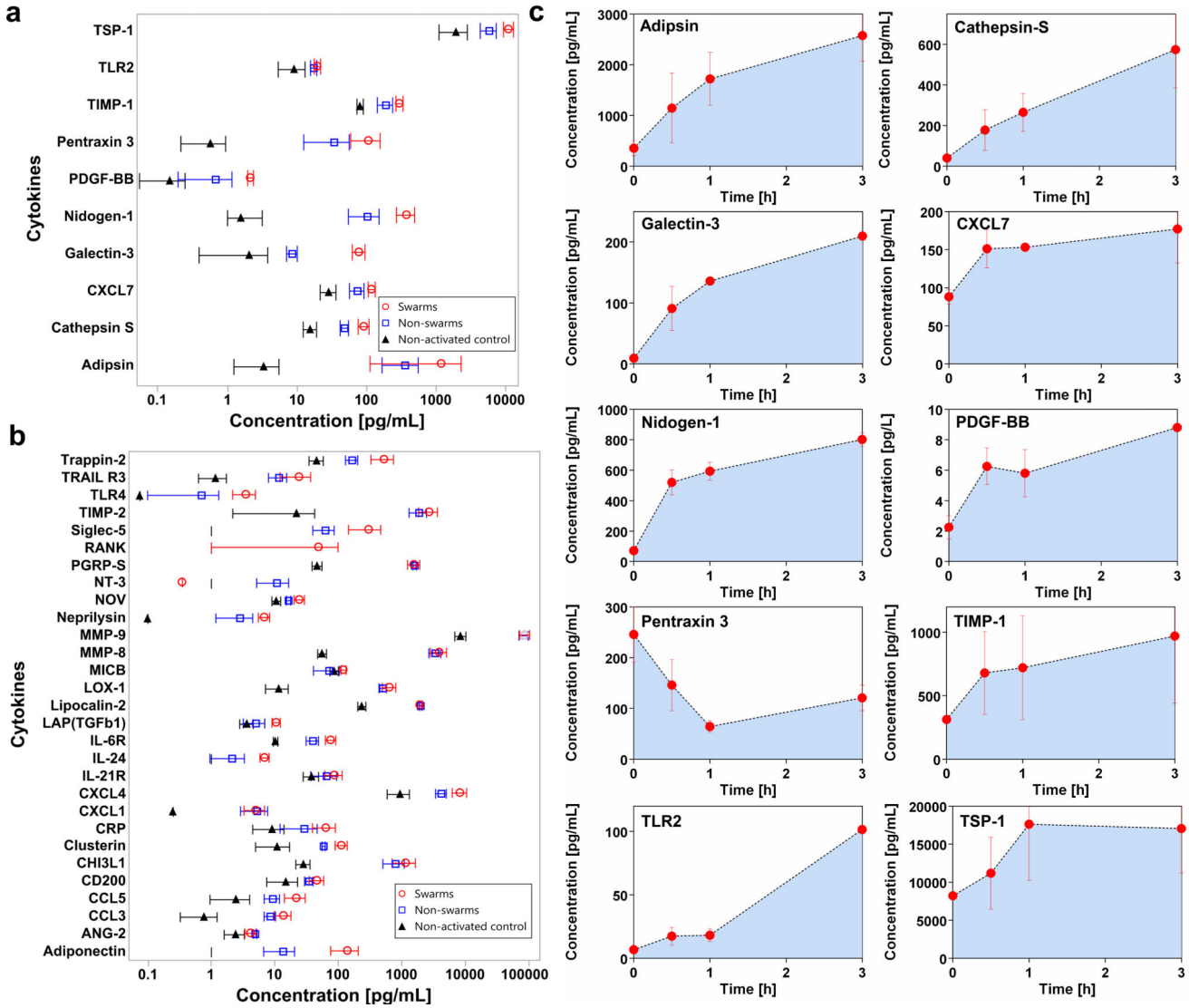

Figure 5. Cytokines released by human neutrophils during swarming

(a) Swarming-specific cytokines released at one hour after the start of swarming have different levels levels during swarming compared to non-swarming and non-activated controls (N = 4 donors, N = 2540 swarms, $p < 0.05$). Please note the logarithmic scale along the concentration axis. **(b)** Quantitative protein microarrays helped identify cytokines released by neutrophils at one hour after the initiation of swarming on zymosan particle clusters. Cytokines that are present in the supernatant at significantly different levels between swarms, non-swarms, and non-activated controls (N = 4 donors, N = 2540 swarms, $p < 0.05$). **(c)** Three distinct temporal profiles for swarming-specific cytokines were identified by comparing supernatants collected at 0, 30, 60 and 180 minutes. Several cytokines increased in concentration over time (e.g. Adipsin, Galectin 3, Nidogen-1, TLR2, Cathepsin-S), some reached a plateau after 90 minutes (e.g. CXCL7, PDGF0BB, TIMP-1, TSP-1), and one decreased over time (Pentraxin-3). Error bars represent standard error of the mean.

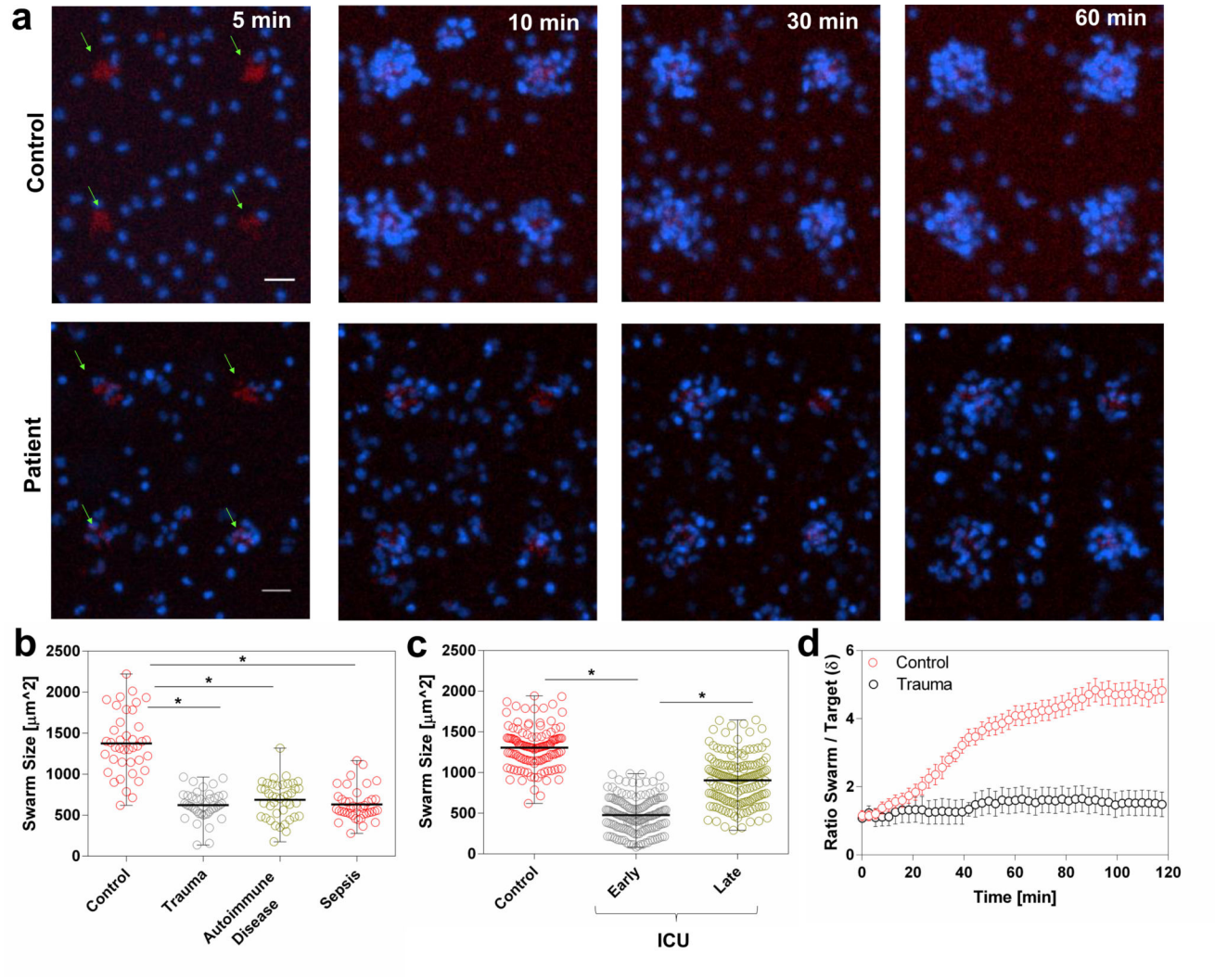

Figure 6. Analysis of clinical samples during neutrophil swarming

(a) Time-lapse fluorescence microscopy images of neutrophils swarming for healthy individuals and patients. Neutrophils from healthy individuals develop stable swarms after 1 h of persistent migration. Neutrophils from patients do migrate persistently towards the zymosan particle targets (green arrows). **(b)** The size of neutrophil swarms is decreased in patients after major trauma, autoimmune diseases, and sepsis. Error bars represent the minimum and maximum value of the experimental group. (N = 4, * $p < 0.05$, Student's *t*-test). **(c)** The size of neutrophil swarms is decreased early in trauma patients compared to controls and recovers over time. Error bars represent the minimum and maximum value of the experimental group (N = 7; * $p < 0.05$, Student's *t*-test). **(d)** Comparison of neutrophil recruitment over time shows that the neutrophils from patients (black) accumulate to swarms slower and the swarms grow at slower rate and reach smaller size compared to healthy controls (red) (N = 2 experiments, N=20 swarms, error bars represent standard error of the mean).